GTD, PO, PTD, AND GAUSSIAN BEAM DIFFRACTION ANALYSIS TECHNIQUES APPLIED TO REFLECTOR ANTENNAS*

INVITED PAPER

Y. RAHMAT-SAMII, P. O. IVERSEN, and D. W. DUAN
Department of Electrical Engineering
University of California, Los Angeles
Los Angeles, CA 90024-1594

ABSTRACT

Several available diffraction analyses techniques are compared in this paper. Techniques including GTD, PO, PTD, and Gaussian Beams, are used to analyze representative reflector antenna geometries. First the techniques are compared for a flat circular disc, representing an unfocused system. Next, the techniques are applied to offset ellipsoidal reflectors and the offset parabolic reflectors. Near-fields, focal-fields and far-fields are determined using these techniques. Both co-polar and cross-polar fields are compared. The acceptability ranges of each technique is carefully investigated. Numerical data are presented for representative configurations and, in particular, field intensities are determined for high power microwave applications.

I Introduction

Reflector antennas continue to be a highly cost and performance competitive alternative for medium to high gain microwave antenna systems. In many modern applications such as satellite communications, beam waveguide fed antennas, compact range measurements, and high power microwave (HPM) systems, accurate and efficient diffraction analysis techniques have become indispensable for effective performance predictions of the radiating system.

The purpose of this paper is to review several of the numerous diffraction techniques (see, for example, [1, 2, 3]) for the analysis of reflector antennas. These techniques include those which have been used extensively for reflector analysis such as (i) Physical Optics (PO) [1], (ii) Geometrical Theory of Diffraction (GTD) [4], (iii) Uniform Asymptotic Theory (UAT) [5, 6], (iv) Uniform Geometrical Theory of Diffraction (UTD) [7], and (v) Theory of Gaussian Beams [8]. A class of Physical Theory of Diffraction (PTD) techniques, which are modifications of Ufimtsev's PTD [9], are also studied: (vi) Mitzner's incremental length diffraction coefficients (ILDC) [10], (vii) Michaeli's equivalent edge currents (EEC) [11], and (viii) Ando's modified physical theory of diffraction [12]. Comparative results are presented for flat circular discs (an unfocused system), offset ellipsoidal reflectors, and offset parabolic reflectors (focused systems).

Most of the earlier literature emphasize the analysis of the radiated far-field of reflector systems. However, a knowledge of the near-fields has become important for recent appli-

*This work was supported in part by U. S. Army Research Grant DAAL02-89-K-0129

cations such as HPM systems, compact range measurements, and multi-reflector antenna designs. This paper presents comparisons among the various techniques for both near-field and far-field scenarios. Extra emphasis will be given to the offset ellipsoidal reflector because of the scant literature describing its characteristics [13].

Although this paper deals only with the conic-section reflectors, all the techniques could equally well be applied to reflectors of arbitrary shape. Furthermore, since many shaped reflectors are perturbations of conic-section reflectors, it is the opinion of the authors that the conclusions drawn about the accuracy and applicability of the various techniques can be extended to shaped reflectors.

II Circular discs

The PTD (physical theory of diffraction) and GTD (geometrical theory of diffraction) techniques listed in Table 1 will be studied in this section by analyzing the scattering from a conducting circular disc of radius a (Fig. 1). The feed is a short dipole located a distance d in front of the disc center. This problem is chosen because it facilitates effective comparisons among various techniques.

II.1 formulation

The PTD techniques that will be studied are modifications of Ufimtsev's physical theory of diffraction [9]. In these techniques, the total scattered field consists of two components, the physical optics (PO) field and the fringe field:

$$\vec{E}^{PTD} = \vec{E}^{PO} + \vec{E}^{fr}. \tag{1}$$

In the far field region, the PO field can be constructed by [1],

$$\vec{E}^{PO} = -j\omega\mu\frac{e^{-jkr}}{4\pi r}(\hat{\hat{1}} - \hat{r}\hat{r}) \cdot \int\int_{\Sigma}(2\hat{n} \times \vec{H}^{i})e^{jk\hat{r}\cdot\vec{r}_{\sigma}}d\sigma, \tag{2}$$

where Σ is the scatterer surface, $\hat{n}$ is a unit normal of the surface, $2\hat{n} \times \vec{H}^{i}$ is the PO current, and $\hat{\hat{1}}$ is the unit dyad. The dyad $(\hat{\hat{1}} - \hat{r}\hat{r})$ serves to extract the transverse (to $\hat{r}$) component of the surface integral. The fringe field is determined by the electric and magnetic equivalent currents along the scatterer edge:

$$\vec{E}^{fr} = -j\omega(\hat{\hat{1}} - \hat{r}\hat{r}) \cdot \vec{A} + jk\hat{r} \times \vec{F} \tag{3}$$

$$\vec{A} = \frac{\mu}{4\pi}\int_{\Gamma}\hat{z}' I^{eq}\frac{e^{-jk|\vec{r}-\vec{r}'|}}{|\vec{r}-\vec{r}'|}dl' \tag{4}$$

$$\vec{F} = \frac{1}{4\pi}\int_{\Gamma}\hat{z}' M^{eq}\frac{e^{-jk|\vec{r}-\vec{r}'|}}{|\vec{r}-\vec{r}'|}dl', \tag{5}$$

where dl' is a differential path length along the scatterer edge Γ. For every point on the scatterer edge a local coordinate system $\hat{x}' - \hat{y}' - \hat{z}'$ is defined (Fig. 1) in a manner that $\hat{z}'$ is along the tangential direction of the edge. Therefore, the vector $\hat{z}'$ in equations (4) and (5) varies along the integration path. The equivalent edge currents I^{eq} and M^{eq} in equations (4),

(5) can be written in terms of the tangential (to scatterer edge) components of the incident field and the diffraction coefficients D_e, D_x, and D_m as

$$I^{eq} = \frac{j2E^i_{z'}}{\omega\mu \sin^2\theta^i} D_e + \frac{j2H^i_{z'}}{k \sin^2\theta^i} D_x \tag{6}$$

$$M^{eq} = \frac{-j2H^i_{z'}}{\omega\epsilon \sin\theta' \sin\theta^i} D_m, \tag{7}$$

where θ^i is associated with the incident direction and θ' is associated with the observation direction, both with respect to the local coordinate system. Mitzner's [10], Michaeli's [11], and Ando's [12] formulations differ in the detailed expressions of the diffraction coefficients.

The total scattered field in Keller's GTD [4] is divided into a geometrical optics (GO) part and a diffracted part. The detailed expressions for these field components can be found in [14, 15]. The singularities of GTD at the shadow boundary (SB) and reflection boundary (RB) are cured by its uniform versions, UTD [7] and UAT [5, 6]. In UTD, Fresnel integrals are incorporated to smooth out the singularities in the diffracted field. Similar Fresnel functions were introduced in UAT to modify the GO field so that the singularities in the diffracted field can be cancelled.

II.2 Numerical results

Computer programs have been developed based on these formulations and computations have been conducted for various disc sizes at different frequencies. The co-polar and cross-polar field components calculated by these techniques will be compared with those obtained from PO and the method of moment (MoM), which is treated numerically exact. In the following, typical numerical results will be demonstrated and discussed. Since Mitzner's solution happens to be the same as Michaeli's solution for this problem, their common solutions will be referred to as the ILDC solutions.

The far-field patterns obtained from various techniques are shown in Fig. 2 for a small disc ($a = 1.5\lambda$, $d = 2.75\lambda$). Several facts can be observed from Fig. 2: (1) Compared to the MoM solution, physical optics predicts the field patterns reasonably well up to 30 degrees. The ignored edge effect in PO can be observed most clearly in the far-angle region. (2) All PTD and GTD techniques predict the dip near $\theta = 47°$ and the side lobe near $\theta = 60°$. (3) There is a RB singularity in the GTD solution, but not in UTD or UAT. All three GTD techniques suffer from the caustic singularity at the boresight. (4) Near $\theta = 90°$, Ando's solution approaches the GTD solutions, which overestimate the actual field levels. (5) ILDC solution follows the MoM solution closely throughout the whole angular range.

In Fig. 3, the far-field patterns are plotted for a large disc ($a = 96\lambda$, $d = 176\lambda$) where the method of moments is not easily applicable. As can be seen, the PTD and GTD techniques agree well except in the last side lobe region. PO solution works well up until 30 degrees, but starts to deviate from all other solutions thereafter.

The cross-polar fields obtained by the various techniques are also examined. Generally, the cross-polar fields are very weak around $\phi = 0°$ and $\phi = 90°$ for symmetric antenna configurations, but become significant at $\phi = 45°$. Most of the observations for the co-polar fields discussed above are true for the cross-polar fields, except that PO predicts very different patterns from those predicted by MoM. This is illustrated in Fig. 4 using $a = 6\lambda$, $d = 11\lambda$. Note that in the PO cross-polar field the first few lobes are not predicted, and

the beating pattern outside the main beam region is "out of phase" with other solutions. Nevertheless, the envelope of the field pattern outside the main beam region predicted by PO is not disparate from others for this large disc.

III Ellipsoidal Reflector

We will next consider an offset ellipsoidal reflector. This reflector is of special interest since it gives us a second focal point . The GTD group have a singularity at a focal point and it is of interest to find how close to the focal point these techniques still yield meaningful results. The reflector will be defined by the intersection of an ellipsoid of revolution with a circular cone emanating from one of the ellipsoid's foci as shown in Fig. 5. This particular way of defining the reflector will lead to the reflector having a planar edge and an elliptical aperture [1].

The feed is located at the focus at $z = -c$. The feed is assumed to be in the far-field of the reflector radiating a linearly polarized wave with a radiation pattern given in terms of the feed (source) coordinate system by

$$\vec{E}(r,\theta,\phi) = A\eta\frac{e^{-jkr}}{r}\begin{cases} \cos^{q_x}\theta\cos\phi\,\hat{\theta} - \cos^{q_y}\theta\sin\phi\,\hat{\phi}, & \text{x-polarized} \\ \cos^{q_y}\theta\sin\phi\,\hat{\theta} + \cos^{q_x}\theta\cos\phi\,\hat{\phi}, & \text{y-polarized} \end{cases} \tag{8}$$

where A is a constant related to the power radiated by the feed, η is the intrinsic impedance of free space, and $q_{x,y}$ is related to the illumination edge taper as follows [16].

$$\mathrm{ET} = -20\log_{10}\left[\cos^{q_{x,y}}\alpha\right] \tag{9}$$

This particular model for the feed is chosen for its simplicity.

The following sections present an outline of the solution approaches for the scattered fields as obtained by the GTD, near-field PO, and Gaussian Beam techniques.

III.1 GTD Solution

The GTD solution is an approximate high frequency solution that is useful in determining the scattered fields of objects that are large compared to a wavelength. For the given incident field produced by the feed the total reflected field at the observation point (P_f) is found through the asymptotic solution given by Keller's Geometrical Theory of Diffraction [4]. As mentioned earlier, this solution can be written in the form

$$\vec{E}(P_f) = \vec{E}_g + \vec{E}_d + O(k^{-1}) \tag{10}$$

where the g-subscript represents the geometrical optics field which is of order k^0. The d-subscript represents the edge-diffracted field which is of order $k^{-1/2}$. These fields can be thought of as "ray fields" that are locally plane waves.

For the ellipsoidal reflector, the problem of locating the reflection point is significantly simplified. This simplification occurs since any ray emanating from one focus will also pass through the other focus. Thus, given an observation point and the location of the focus through which the reflected ray travels, one has two points which define a line. The intersection of this line with the ellipsoid defines the reflection point.

To specify the reflected field one needs the radii of curvatures of the reflected rays. We know that the ellipsoid, according to the GO approximation, will focus all the energy through

the second focus. Thus both principal radii of curvatures of the reflected ray at the reflection point are equal to the distance from the reflection point to the focus F_2.

The geometrical optics field at the reflection point is found through the application of Snell's law. In terms of the incident field unit vector, the reflected field unit vector is given as

$$\hat{e}_r = -\hat{e}_i + 2(\hat{n}_\Sigma \cdot \hat{e}_i)\hat{n}_\Sigma \tag{11}$$

The unit vector $\hat{e_r}$ gives the direction of the electric field for the reflected ray. The vector $\hat{n_\Sigma}$ is the unit normal to the surface at the reflection point. The reflected field can for our geometry be written as follows

$$\vec{E}_g(P_f) = \frac{A\eta \exp[-jk(d_1+d_2)]}{1-d_2/R}\,\hat{e}_r \tag{12}$$

where d_1 and d_2 are the distances from the feed to the reflection point and from the reflection point to the observation point , respectively. R is the radii of curvature of the reflected field at the reflection point. Notice that the magnitude of the field will become infinite when the observation point is at the focus ($d_2 = R$). Further, notice the phase shift of 180° that occurs when the ray passes through the focus. This phase shift has been discussed extensively in the literature and is known as the Phase Anomaly or Gouy's phase shift after the French scientist who first discovered it.

The edge-diffracted field is due to the contribution from diffraction points lying on the edge of the reflector. These diffraction points are found through the application of the law of edge diffraction. The total diffracted field is found by summing up the contribution from all of the diffraction points. The diffracted field is given by the expression [4]

$$\vec{E}(x,y,z) \;=\; g(kd_4)\mathrm{DF}\frac{1}{\sin\theta_i}[D_s E^i_\theta\,\hat{\theta} + D_h E^i_\phi\,\hat{\phi}] \tag{13}$$

in which $g(kd_4)$ is a cylindrical wave factor, DF is the divergence factor, and $D_{s,h}$ are the soft and hard diffraction coefficients. Detailed expression for each of these terms can be found in the literature [14, 15].

III.2 Physical Optics Solution

In a scattering problem we can find the scattered *near-field* from the integral representations

$$\vec{E} \;=\; -j\omega\mu\int_\Sigma \left[\vec{J}g + \frac{1}{k^2}(\vec{J}\cdot\nabla)\nabla g\right] dS' \tag{14}$$

$$\vec{H} \;=\; \int_\Sigma [\vec{J}\times\nabla g]\,dS' \tag{15}$$

where $\vec{J}$ is the induced current on the scatterer and g is the free-space Green's function given by

$$g \;=\; \frac{e^{-jkR}}{4\pi R} \tag{16}$$

$$R \;=\; |\vec{r}-\vec{r}\,'| \tag{17}$$

and Σ is the surface of the scatterer. These equations can be derived through the Stratton-Chu formulation [17]. The Physical Optics method (PO) assumes that the scatterer is an

infinite ground plane and thus, assumes $\vec{J}$ to be given by

$$\vec{J} = 2\hat{n} \times \vec{H}^i \tag{18}$$

where $\hat{n}$ is the normal to the surface and $\vec{H}^i$ is the incident H-field. This approximation for $\vec{J}$ has been shown to be useful for relatively large and smooth scatterers. The accuracy of this approximation becomes questionable near the edges of the scatterer since the PO current does not satisfy the Meixner edge condition . The PTD techniques described in the previous section attempt to compensate for this deficiency. Although we will not present the PTD solutions for this reflector, the techniques are applicable for the analysis of reflector antennas [18, 19]. A computer program was written that numerically evaluates the integrals in Eq. (14) and (15) using two-dimensional nine-point Gaussian quadrature and subsectioning.

III.3 Gaussian Beam Solution

A method frequently used for the solution of beam waveguide and lens problems is the theory of Gaussian beams. Gaussian beams are a result of an approximate analytic solution to the wave equation. We assume that the beam consists of field components purely transverse to the direction of propagation and that the phase varies essentially as a plane wave. That is, we look for solutions to the scalar wave equation of the form.

$$E(x,y,z) = E_o \psi(x,y,z) e^{-jkz} \tag{19}$$

The factor $\psi(x,y,z)$ describes how the beam deviates from a plane wave. Substitution of Eq.(19) in the wave equation and assuming a paraxial beam, we find the fundamental Gaussian mode which is given in cylindrical coordinates by

$$\psi(r,z) = \sqrt{\frac{2}{\pi}} \frac{1}{w(z)} \exp\left[\frac{-r^2}{w^2(z)} - j\left(\frac{-kr^2}{2R^2(z)} - \Phi(z)\right)\right] \tag{20}$$

where R(z),w(z) and Φ(z) are defined as

$$R(z) = z\left[1 + (\frac{\pi w_o^2}{\lambda z})^2\right] \tag{21}$$

$$w^2(z) = w_o^2\left[1 + (\frac{\pi w_o^2}{\lambda z})^2\right] \tag{22}$$

$$\Phi(z) = \arctan\left[\frac{\lambda z}{\pi w_o^2}\right] \tag{23}$$

The first term in the exponent is a radial amplitude factor, the second term is a radial phase factor, and the last two terms are longitudinal phase factors. The term w(z) is called the beam width and gives the radius at which the field has fallen off to a value of e^{-1} times the value on the axis. The term R(z) is the radius of curvature of the phase front. Fig. 7 illustrates the propagation of a Gaussian beam.

In order to compare the Gaussian beam solution with the PO and GTD solutions, we have to specify the feed pattern in the same fashion. That is, we have to relate the $\cos^q(\theta)$ feed pattern to a Gaussian beam. We can determine the beam waist and its location for the

equivalent incident Gaussian beam by equating the radius of curvature, and the e^{-1} point of the $\cos^q(\theta)$ pattern to that of the incident Gaussian beam.

Using the assumptions of Gaussian beam propagation we can replace the ellipsoid with an equivalent lens of focal length f given by [8]

$$\frac{1}{f} = \frac{1}{d_1} + \frac{1}{d_2} \tag{24}$$

in which $d_{1,2}$ are the distances from the focal points $F_{1,2}$ to the reflection point for the central ray of the incident beam. The reflected beam is found through the transformation in radii of curvature as the beam passes through the equivalent lens. The beam width is assumed to be unchanged passing through the lens. It can be shown that the beam waist of the transformed beam is given by the equation

$$w_{o2} = \frac{w_{o1}}{\sqrt{(d_1/f - 1)^2 + (\frac{\pi w_{o1}^2}{\lambda f})^2}} \tag{25}$$

where w_{o1} and w_{o2} are the waists of the incident and reflected beams, respectively. Further, the location of the waist is given by

$$z_2 = f\left[1 + \frac{z_1/f - 1}{(z_1/f)^2 + (\frac{\pi w_{o1}^2}{\lambda f})^2}\right] \tag{26}$$

in which $z_{1,2}$ are the axial distances from the reflector to the beam waists for the incident and reflected beams. Given the location and size of the waist of the Gaussian beam, together with the direction of the central axis, we can evaluate the scattered field.

III.4 A Generic Offset Ellipsoidal Reflector

Let us choose an ellipsoid given by $a = 40\lambda$ and $b = 50\lambda$. This ellipsoid has focal length, $f = 20\lambda$ and eccentricity, $e = 0.6$. Consider a reflector produced by specifying $\beta = 5\pi/6$, $\alpha = \pi/12$. Referring to the geometry of Fig. 5, these specifications lead to a reflector with an elliptical aperture described by $a' = 19.73\lambda$, and $b' = 16.85\lambda$. Such a reflector could conceivably be used in a beam waveguide or a Gregorian antenna system. Having specified the reflector, we also need to define the feed of this system. We choose to investigate the case of a feed pointing towards the center of the reflector as seen from the feed. The taper of the feed is determined by the choice of q_x and q_y. For the particular value of α chosen, a value of $q_x = q_y = 50$ will lead to a feed edge taper (ET) of $-20\log[\cos^{50}(\alpha)] = 15.06$ dB.

Figs. 8-9 show the magnitudes and phases for the dominant components of the E-field along the central reflected ray, as obtained using the GTD, PO and Gaussian Beam methods. We see that away from the focal point in the main beam direction, the GTD and Gaussian Beam solutions both give results that are very close to the PO solution. Near the focal point both the Gaussian Beam and the GTD methods predict erroneous results for the magnitude. The Gaussian Beam method predicts a phase that is very close to that predicted by PO even though the magnitude differs. Notice also that the GTD solution displays the same sort of ripple as the PO solution in both its magnitude and phase.

Let us graph the magnitude of the fields of this reflector in a line that is perpendicular to the reflected ray and lies on the x-z plane. Fig. 10 shows the magnitude of the E-field

along this line. Notice that the fields are given in terms of dB Volts/wavelength. These units are defined as $20\log_{10}[E(\text{Volts/wavelength})]$. We see that the Gaussian Beam solution is close to the PO solution around the focal point, but becomes drastically erroneous as one moves away from the focal point in the direction transverse to the main beam direction. The GTD solution is in error close to the focal point, but it provides accurate results away from the focal point. We see that with a prudent combination of the GTD and Gaussian Beam methods one could establish a correct field distribution in the focal region while avoiding the time consuming PO integration.

III.5 Effects of Varying the Geometry

The accuracy of the various approximate techniques is strongly problem dependent. The problem described in Figs. 8 and 9 is a highly focused system. That is, the subtended angles are large. For this system the GTD solution is accurate to within a few wavelengths from the second focal point. Consider now a geometry with much smaller subtended angles. Figs. 11 and 12 show the scattered magnitude and phase along the central reflected ray of a system where $\beta = \pi/6$ and $\alpha = \pi/12$. As can be observed the GTD solution is in this case in error over a region covering ten's of wavelengths. The Gaussian Beam solution follows the PO solution relatively closely. This is expected, since the Gaussian Beams are based on a paraxial approximation.

Figs. 13 and 14 shows the magnitude and phase of the scattered field for the case where the reflector is relatively large, and the feed edge taper is very high, 45dB (low edge illumination). In this case we see that the Gaussian Beam solution tracks the PO solution very closely.

III.6 Regions of Validity of the GTD and Gaussian Beam Methods

It is apparent from the previous sections that a combination of the fundamental mode Gaussian Beam method and the GTD method can, in many cases, give an accurate description of the caustic region fields of an offset ellipsoidal reflector. The difficulty lies in determining in which exact regions and for what type of geometries each of the methods provide good results. Let us try to provide some general guidelines. The Gaussian Beam solution will give good results as long as the assumptions made in the derivation of the Gaussian beams are not violated. That is, the divergence angles should be small, less than approximately 30 degrees. Further, the beams should have beam widths of the order of λ or greater. Finally, the edge taper should be large (low edge illumination) so that the truncation of the Gaussian Beam will not affect the results significantly. When the divergence angles are large, the Gaussian Beam method approaches the GO solution and it becomes erroneous near the focal point.

There are three major drawbacks of the Gaussian Beam approach. First, since it is a scalar analysis it contains no information with regards to the cross-polarized fields. Second, it fails when the observation point is more than a few beamwidths into the geometrical shadow region, even for edge tapers that are relatively large. Third, the Gaussian Beam solution is not easily modified to account for feed displacements, and for patterns that are not circularly symmetric. It should be mentioned that the inclusion of higher order Gaussian modes can mend the second deficiency.

The GTD solution although failing at the focal point, gives accurate results for both magnitude and phase as long as the angle subtended by the reflector at F_2 is large. For this situation the location of maximum field strength is close to F_2 which is what GTD

predicts. The GTD solution gives accurate result in shadow regions and does contain information about the cross-polarized components. Its accuracy in the focal region increases with increased edge illumination.

There are two major drawbacks of the GTD solution. First, it is not valid at or close to the focal point. Second, it is not able to predict correct results even far from the focal point when the reflector is small or the subtended angles are small (less than about 30°). That is, it does not predict any defocusing. Given a specific reflector one needs to keep in mind the above mentioned limitations of the approximate methods in order to obtain an accurate picture of the field distribution. If the edge tapers are low and the subtended angles are large then the GTD solution will yield results that are accurate everywhere except very close to the focal point (less than a few wavelengths from the focal point). For a reflector of this type the GTD solution will yield more information than the Gaussian Beam solution. The Gaussian Beam method as presented here will not be able to predict the focal field strength for this type of reflector. However, for a reflector with small subtended angles the GTD solution fails everywhere except for very close to or very far from the reflector. For this type of reflector the Gaussian Beam results should be used.

IV Parabolic Reflector

The same computer programs that were developed to analyze the offset ellipsoidal reflector can be applied to the analysis of an offset parabolic reflector by letting the eccentricity of the ellipsoid approach unity. The scattered near-field, far-field, and Fresnel-fields obtained by these techniques have been compared in order to obtain some information about the relative accuracy of the various techniques for this geometry. Fig. 15 shows the far-field radiation pattern of an offset reflector with F/D=1 and a diameter of 30λ. We see that as was the case for the circular disc, the GTD technique fails drastically along the boresight direction but gives reasonable accurate patterns past the first sidelobe. In this case the failure of the GTD technique is "three-fold", since in the boresight direction we have caustics for both the GO field and the diffracted field, and additionally, this is also the direction of the shadow boundaries. Notice that the GTD solution fails on the shadow boundaries. The use of the uniform theories (UAT, UTD) would eliminate this problem. The fundamental order Gaussian beam solution gives a reasonable value for the peak of the main beam but does not predict any sidelobes. Figures 16 and 17 show the Fresnel-field and near-field radiation patterns of the same reflector system.

For certain applications such as high power microwave (HPM) applications there is a need to know the near-field power density, in order to predict maximum power levels limited by air breakdown. Fig. 18 shows a plot of the scattered near-field power density of an offset parabolic reflector that has a feed radiating a total average power of 1 GW at 1 GHz. Fig. 19 shows the total field (scattered plus incident) for the same system. Notice the standing wave that occurs in front of the reflector. It can be seen from Fig. 19 that if we assume that the air breakdown occurs at a field strength of 10^6 V/m, then the total field in front of the reflector could exceed the breakdown field strength.

V Conclusions

In this paper, several of the existing diffraction analysis techniques including GTD, PO, PTD, and Gaussian Beams were applied to representative reflector geometries. The scattered fields in the near-field, focal-field, and far-field regions were determined for various reflectors using these techniques, and both co-polar and cross-polar field components were considered. The ranges of acceptability of each technique was carefully identified. Numerical results were presented to illustrate comparatively the accuracy and applicability of each of these techniques. Also, field intensities were determined for high power microwave (HPM) applications. The GTD and PO/PTD techniques were applied to circular discs and it was found that Mitzner and Michaeli's solution provide the most accurate fit to the MoM solution. GTD, PO and Gaussian Beam techniques were applied to offset parabolic and offset ellipsoidal reflectors and it was found that in many cases a combination of the fundamental mode Gaussian Beam technique and the GTD technique can yield accurate representations of the scattered field, thus avoiding the sometimes very time consuming PO integration.

The results demonstrated in this paper gave useful suggestions and justifications for the applicability of each technique in applications such as satellite communications antennas, beam waveguide fed antennas, compact antenna range measurements, and high power microwave (HPM) systems, where accurate near- and far-field predictions are required.

References

[1] Y. Rahmat-Samii. "Reflector antennas". In Y. T. Lo and S-W Lee, editors, *"Antenna Handbook"*, chapter 15. Van Nostrand Reinhold Company, New York, 1988.

[2] W. V. T. Rusch. "The current state of the reflector antenna art". *IEEE Trans. Antennas Propagat.*, AP-32(4):313–329, April 1984.

[3] A. W. Love, editor. *"Reflector antennas"*. IEEE Press, New York, 1978.

[4] J. B. Keller. "Geometrical theory of diffraction". *J. Opt. Soc. of America*, 52(2):116–130, Feb. 1962.

[5] D. S. Ahluwalia, R. M. Lewis, and J. Boersma. "Uniform asymptotic theory of diffraction by a plane screen". *SIAM J. Appl. Math.*, 16:783–807, 1968.

[6] S-W Lee and G. A. Deschamps. "A uniform asymptotic theory of electromagnetic diffraction by a curved wedge". *IEEE Trans. Antennas Propagat.*, AP-24(1):25–34, Jan. 1976.

[7] R. G. Kouyoumjian and P. H. Pathak. "A uniform geometrical theory of diffraction for an edge in a perfectly conducting surface". *Proc. IEEE*, 62:1448–1461, Nov. 1974.

[8] T. S. Chu. "An imaging beam waveguide feed". *IEEE Trans. Antennas Propagat.*, AP-31:614–619, July 1983.

[9] P. Y. Ufimtsev. "Method of edge waves in the physical theory of diffraction". *Izd-Vo Sovyetskoye Radio*, pages 1–243, 1962. Translation prepared by the U. S. Air Force Foreign Technology Division Wright-Patterson, AFB, Ohio (1971), available from NTIS, Springfield, VA22161, AD733203.

[10] K. M. Mitzner. "Incremental length diffraction coefficients". Technical Report AFAL-TR-73-296, Aircraft Division Northrop Corp., April 1974.

[11] A. Michaeli. "Elimination of infinities in equivalent edge currents, part I: Fringe current components". *IEEE Trans. Antennas Propagat.*, AP-34(7):912–918, July 1986.

[12] M. Ando. "Radiation pattern analysis of reflector antennas". *Electronics and Communications in Japan, Part 1*, 68(4):93–102, 1985.

[13] R. L. Fante. "An analysis of the elliptical reflector". *IEEE Trans. Antennas Propagat.*, AP-27(4):455–459, July 1979.

[14] S-W Lee. "Uniform asymptotic theory of electromagnetic edge diffraction: a review". In P. L. E. Uslenghi, editor, *Electromagnetic scattering*, pages 67–119. Academic Press, 1978.

[15] Y. Rahmat-Samii and R. Mittra. "Spectral analysis of high frequency diffraction of an arbitrary incident field by a half plane – comparison with four asymptotic techniques". *Radio Science*, 13(1):31–48, Jan.-Feb. 1978.

[16] Y. Rahmat-Samii, P. Cramer, Jr., K. Woo, and S-W Lee. "Realizable feed-element patterns for multibeam reflector antenna analysis". *IEEE Trans. Antennas Propagat.*, AP-29:961–963, Nov. 1981.

[17] R. S. Elliott. *"Antenna theory and design"*. Prentice-Hall, 1981.

[18] V. Hombach and E. Kuhn. "Complete dual-offset reflector antenna analysis including near-field, paint-layer and CFRP-structure effects.". *IEEE Trans. Antennas Propagat.*, 37(9):1093–1101, Sept. 1989.

[19] M. Ando. "PO and PTD analyses of offset reflector antenna patterns". In *1988 IEEE AP-S International Symposium*, pages 112–115. IEEE, 1988.

Table 1: PTD and GTD techniques studied for circular discs.

PTD techniques	
ILDC:	Mitzner's incremental length diffraction coefficients [10].
EEC:	Michaeli's equivalent edge currents [11].
Ando:	Ando's modified physical theory of diffraction [12].
GTD techniques	
GTD:	Geometrical Theory of Diffraction [4].
UTD:	Uniform Geometrical Theory of Diffraction [7].
UAT:	Uniform Asymptotic Theory [5, 6].

Captions:

Fig. 1: Geometry of the disc-dipole radiation system.

Fig. 2: Co-polar far-field patterns ($\phi = 0°$) for a circular disc of radius $a = 1.5\lambda$ and a disc-dipole distance $d = 2.75\lambda$. (All curves normalized to boresight PO field.)

Fig. 3: Co-polar far-field patterns ($\phi = 0°$) for a circular disc of radius $a = 96\lambda$ and a disc-dipole distance $d = 176\lambda$. (All curves normalized to boresight PO field.)

Fig. 4: Cross-polar far-field patterns ($\phi = 45°$) for a circular disc of radius $a = 12\lambda$ and a disc-dipole distance $d = 22\lambda$. (All curves normalized to boresight co-polar PO field.)

Fig. 5: Offset ellipsoidal reflector geometry.

Fig. 6: Rays contributing to the scattered field for the GTD solution.

Fig. 7: Propagation of a Gaussian Beam.

Fig. 8: $|E_y|$ along the central reflected ray for an offset ellipsoidal reflector with $b = 50\lambda$, $a = 40\lambda$, $\beta = 5\pi/6$, $\alpha = \pi/12$, and a y-polarized feed with ET = 15 dB.

Fig. 9: Phase of E_y (in degrees) normalized to $\exp[-jk(d_1 + d_2)]$ for a reflector with $b = 50\lambda$, $a = 40\lambda$, $\beta = 5\pi/6$, $\alpha = \pi/12$, and a y-polarized feed with ET = 15 dB.

Fig. 10: $|E_y|$ along a line perpendicular to the central reflected ray for an offset ellipsoidal reflector with $b = 50\lambda$, $a = 40\lambda$, $\beta = 5\pi/6$, $\alpha = \pi/12$, and a y-polarized feed with ET = 15 dB.

Fig. 11: $|E_y|$ along the central reflected ray for an offset ellipsoidal reflector with $b = 50\lambda$, $a = 40\lambda$, $\beta = \pi/6$, $\alpha = \pi/12$, and a y-polarized feed with ET = 15 dB.

Fig. 12: Phase of E_y (in degrees) normalized to $\exp[-jk(d_1 + d_2)]$ for a reflector with $b = 50\lambda$, $a = 40\lambda$, $\beta = \pi/6$, $\alpha = \pi/12$, and a y-polarized feed with ET = 15 dB.

Fig. 13: $|E_y|$ along the central reflected ray for an offset ellipsoidal reflector with $b = 100\lambda$, $a = 80\lambda$, $\beta = 5\pi/6$, $\alpha = \pi/12$, and a y-polarized feed with ET = 45 dB.

Fig. 14: Phase of E_y (in degrees) normalized to $\exp[-jk(d_1 + d_2)]$ for a reflector with $b = 100\lambda$, $a = 80\lambda$, $\beta = 5\pi/6$, $\alpha = \pi/12$, and a y-polarized feed with ET = 45 dB.

Fig. 15: Far-field ($R = 1000\lambda$) co-polarized pattern of an offset parabolic reflector with $F/D = 1$ and $D = 10\lambda$ and with a feed radiating 1 kW of power, having an edge taper of 10 dB.

Fig. 16: Fresnel-field ($R = 50\lambda$) co-polarized pattern of an offset parabolic reflector with $F/D = 1$ and $D = 10\lambda$ and with a feed radiating 1 kW of power, having an edge taper of 10 dB.

Fig. 17: Near-field ($R = 20\lambda$) co-polarized pattern of an offset parabolic reflector with $F/D = 1$ and $D = 10\lambda$ and with a feed radiating 1 kW of power, having an edge taper of 10 dB.

Fig. 18: Scattered near-field of an offset parabolic reflector with $F/D = 1$ and $D = 3$m and with a feed radiating 1 GW of power at 1 GHz, having an edge taper of 10 dB.

Fig. 19: Total (scattered plus incident) near-field of an offset parabolic reflector with $F/D = 1$ and $D = 3$m and with a feed radiating 1 GW of power at 1 GHz, having an edge taper of 10 dB.

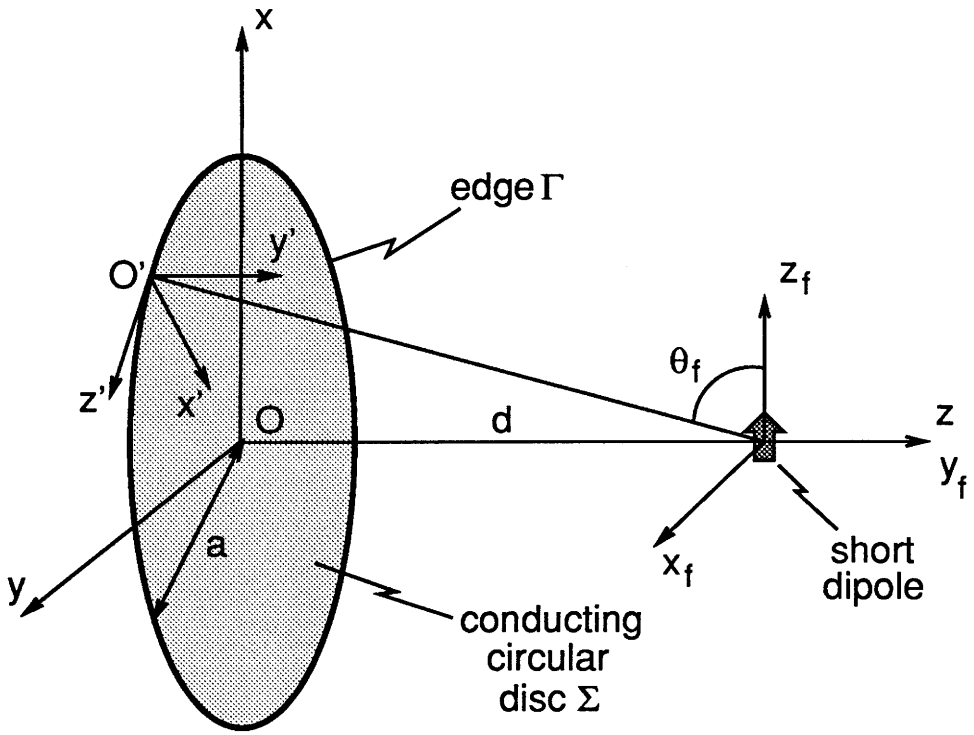
x
edge Γ
y'
O'
z'
x'
O
d
z_f
θ_f
z
y_f
x_f
short
dipole
a
y
conducting
circular
disc Σ

Fig. 1

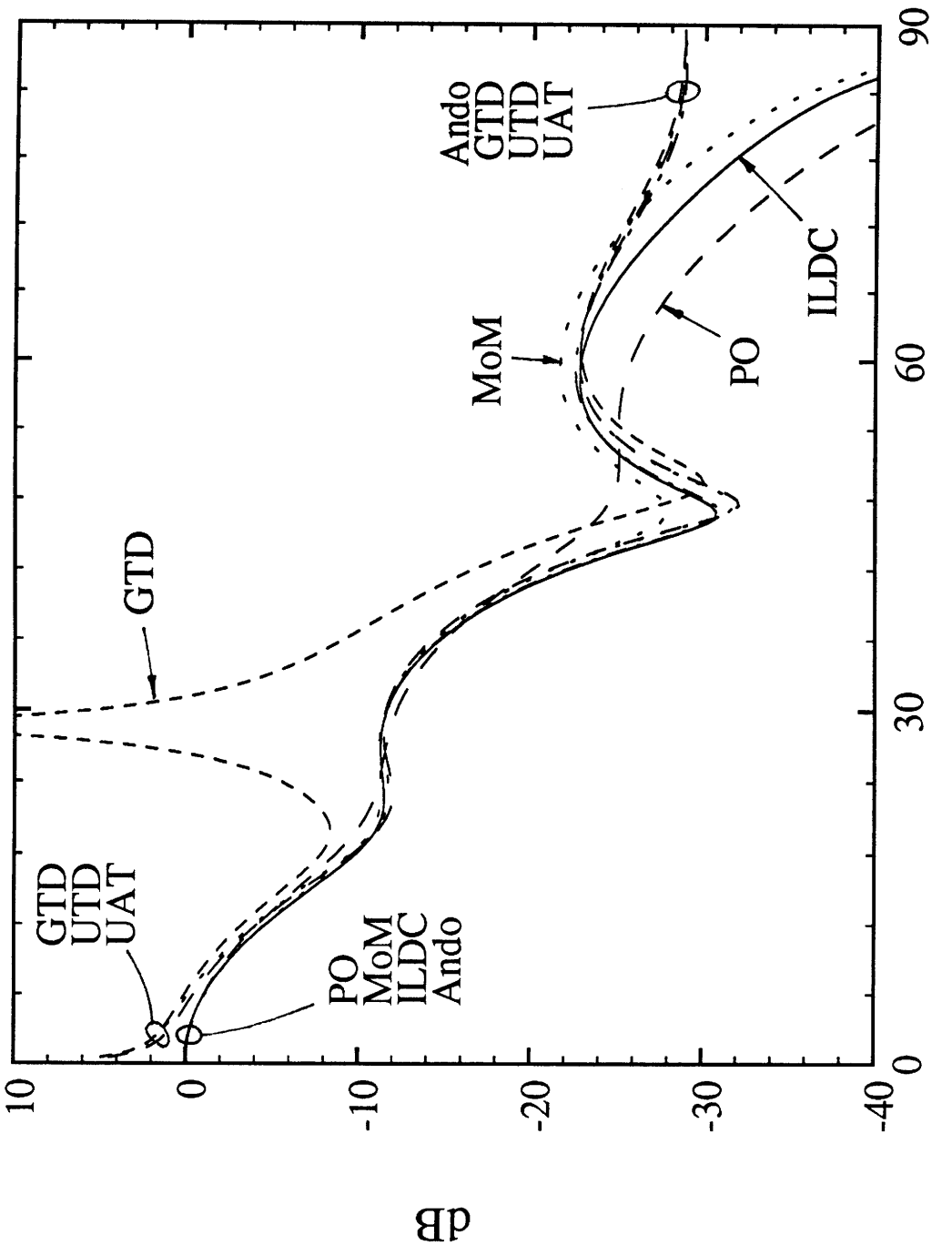
dB
10
0
-10
-20
-30
-40
0
30
60
90
θ (deg)
GTD
UTD
UAT
GTD
PO
MoM
ILDC
Ando
Ando
GTD
UTD
UAT
MoM
PO
ILDC

Fig. 2

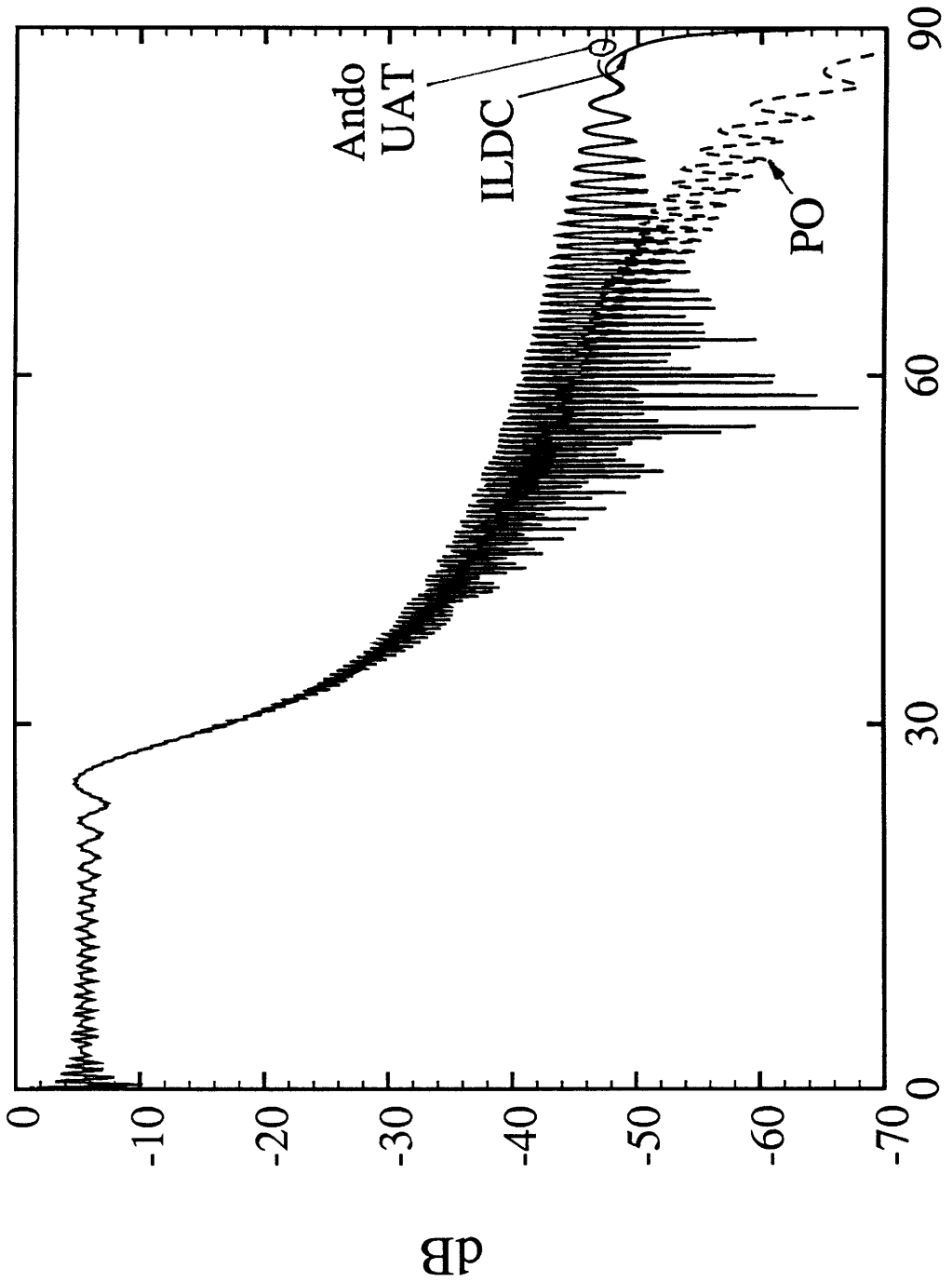

Fig. 3

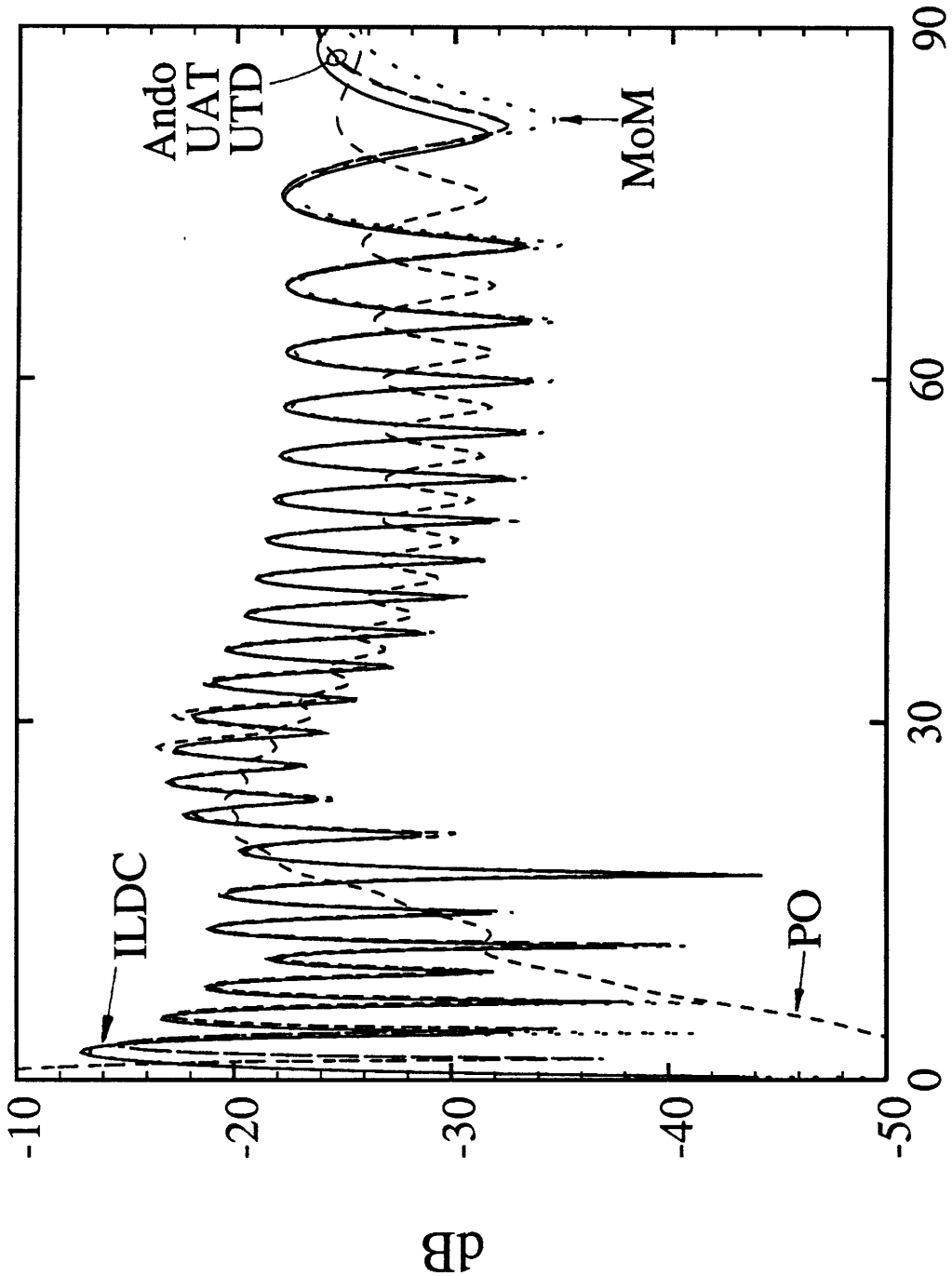

Fig. 4

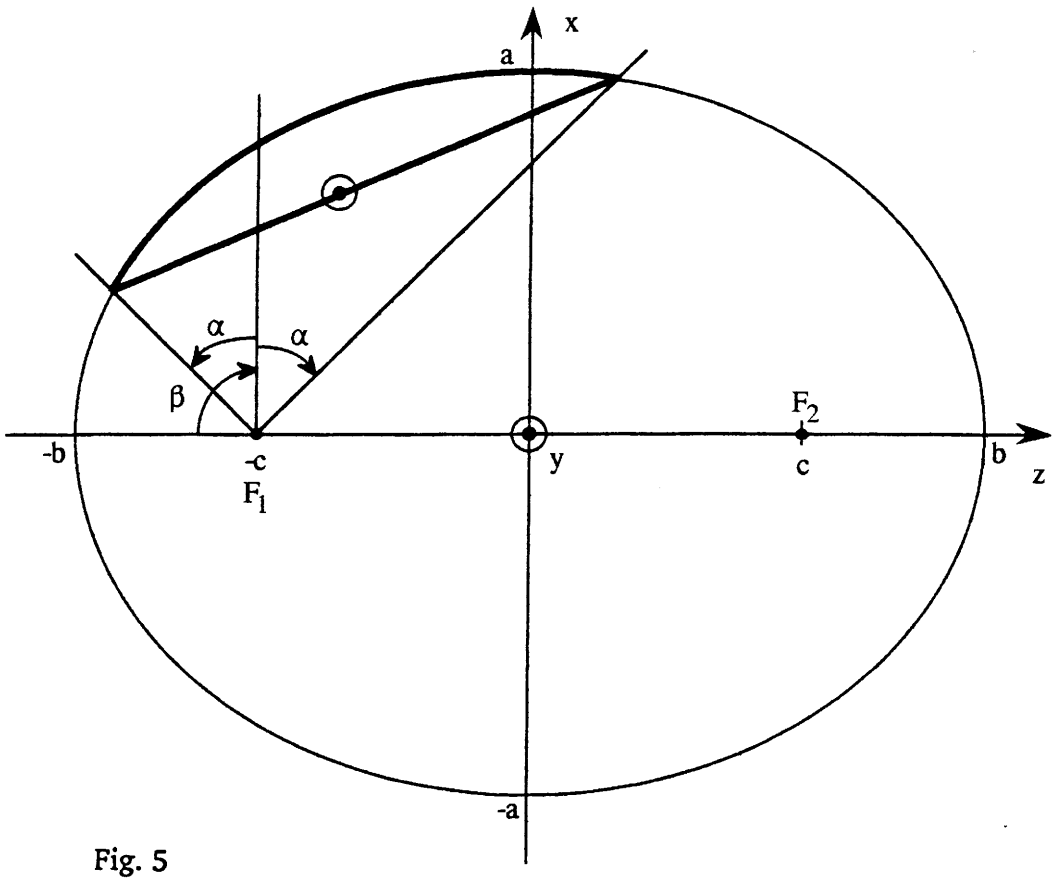
x
a
α
α
β
F2
-b
-c
F1
y
c
b
z
-a

Fig. 5

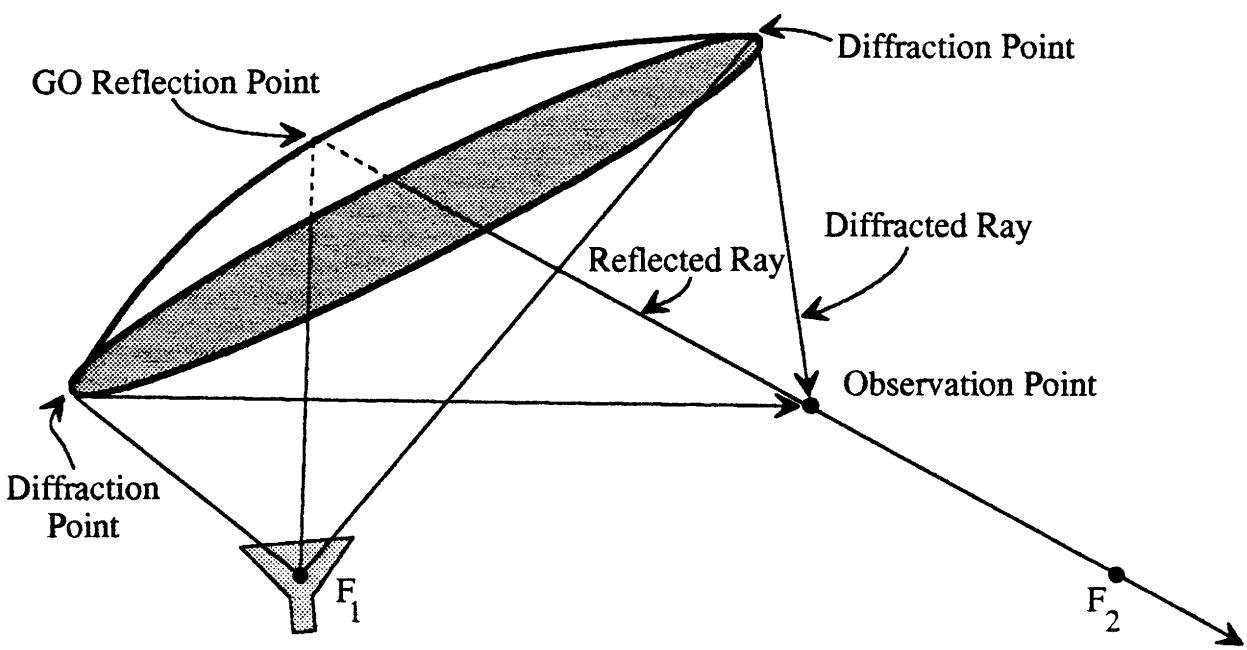
Diffraction Point
GO Reflection Point
Diffracted Ray
Reflected Ray
Observation Point
Diffraction
Point
F1
F2

Fig. 6

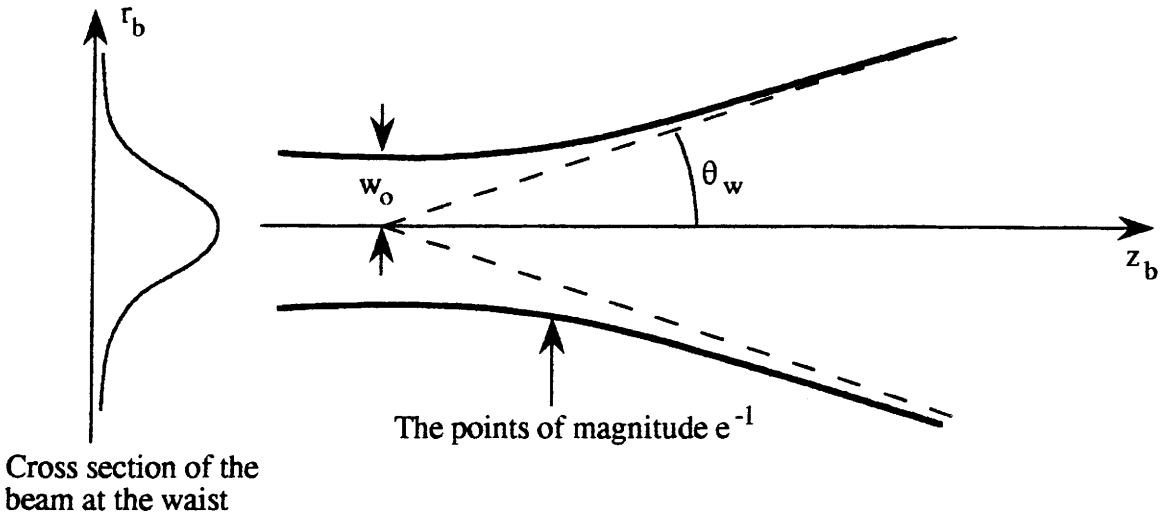
r_b
w_o
θ_w
z_b
The points of magnitude e^{-1}
Cross section of the beam at the waist

Fig. 7

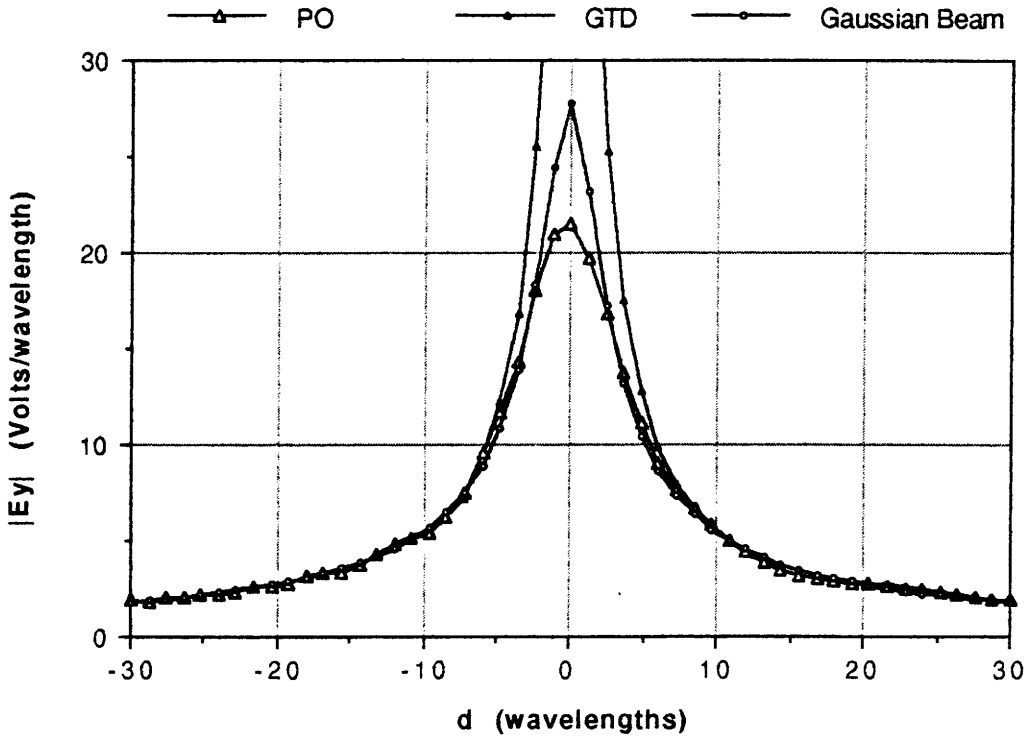
PO
GTD
Gaussian Beam
30
20
10
0
-30
-20
-10
0
10
20
30
|Ey| (Volts/wavelength)
d (wavelengths)

Fig. 8

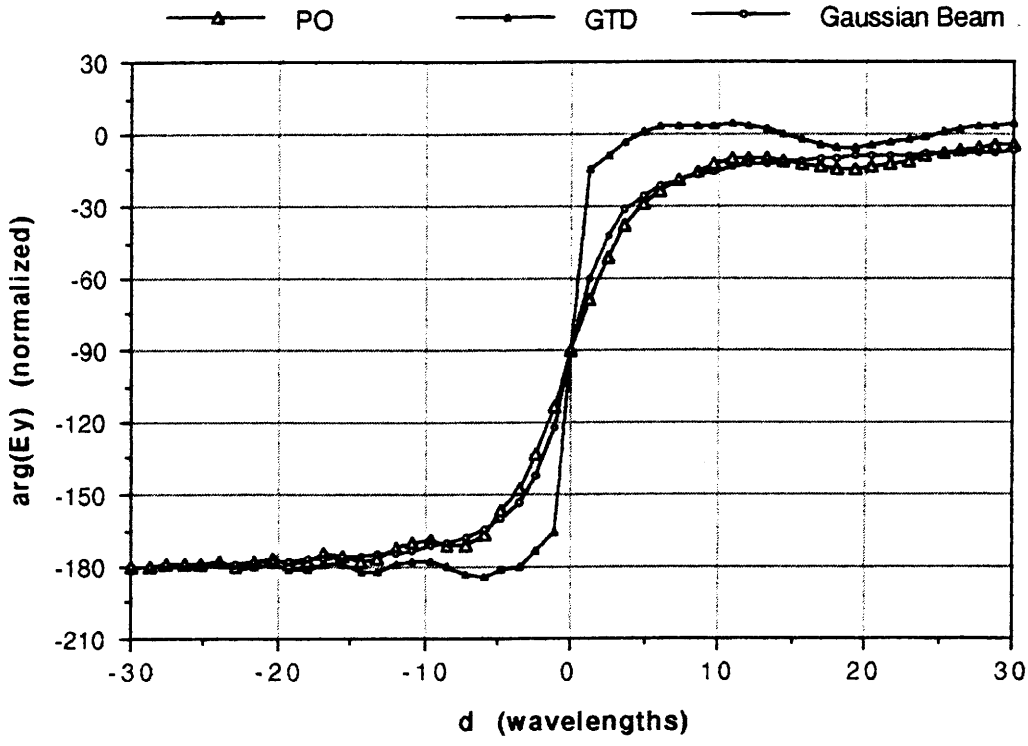
PO
GTD
Gaussian Beam
30
0
-30
-60
-90
-120
-150
-180
-210
arg(Ey) (normalized)
-30
-20
-10
0
10
20
30
d (wavelengths)

Fig. 9

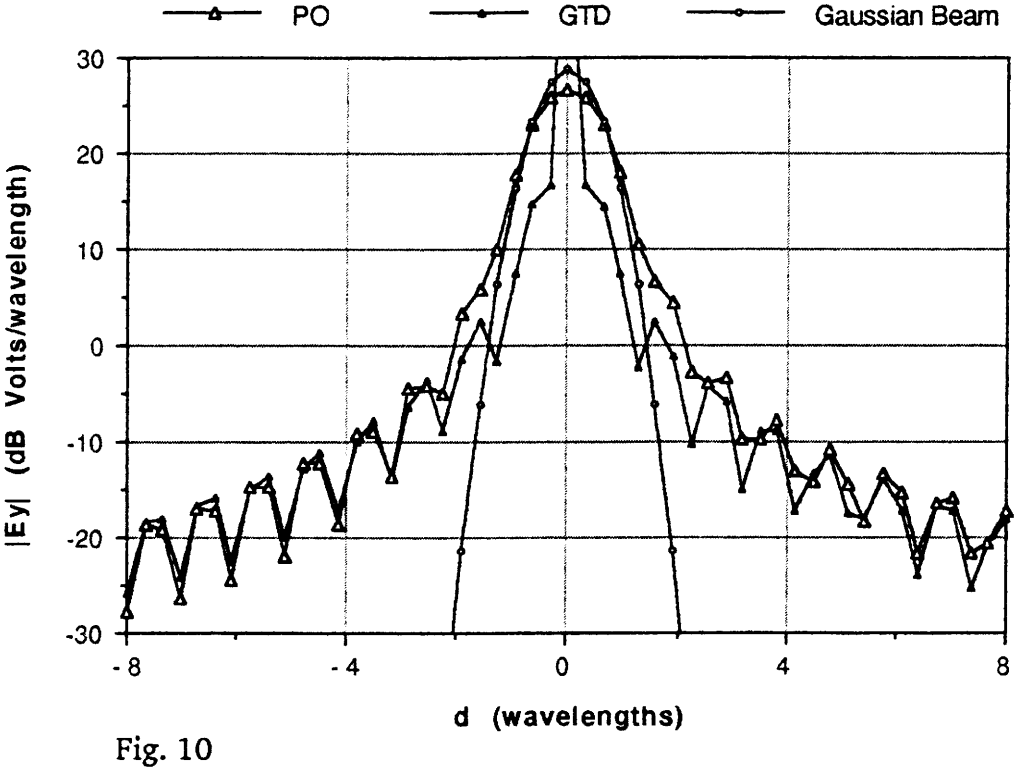
PO
GTD
Gaussian Beam
30
20
10
0
-10
-20
-30
|Ey| (dB Volts/wavelength)
-8
-4
0
4
8
d (wavelengths)

Fig. 10

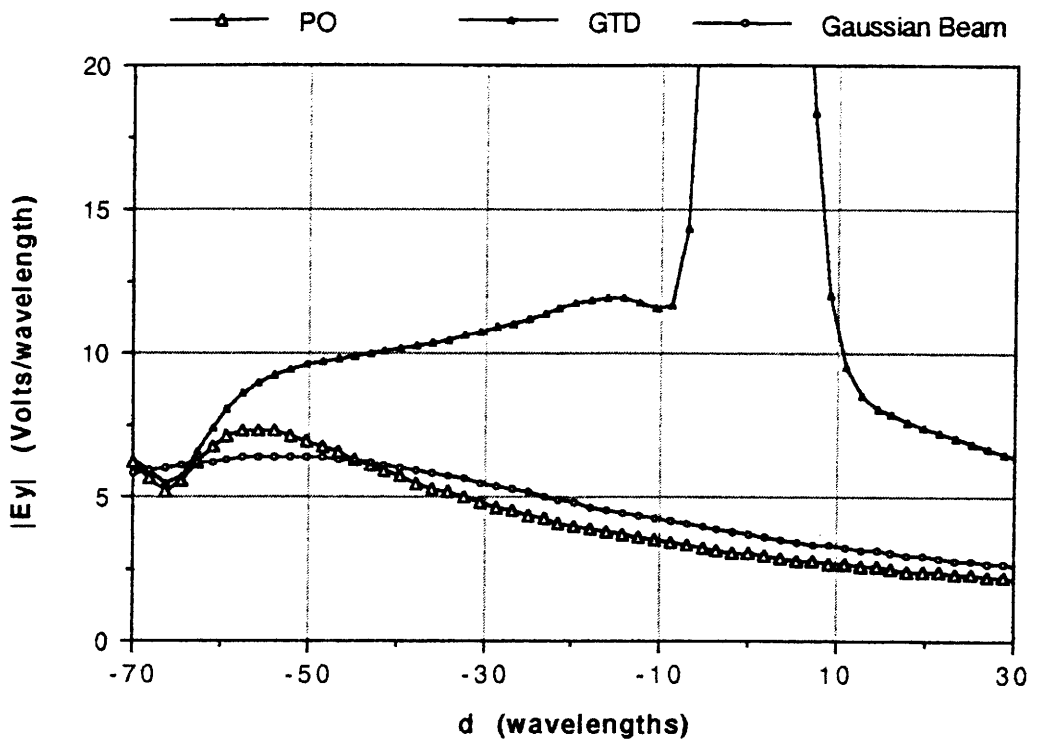
PO
GTD
Gaussian Beam
20
15
10
5
0
|Ey| (Volts/wavelength)
-70
-50
-30
-10
10
30
d (wavelengths)

Fig. 11

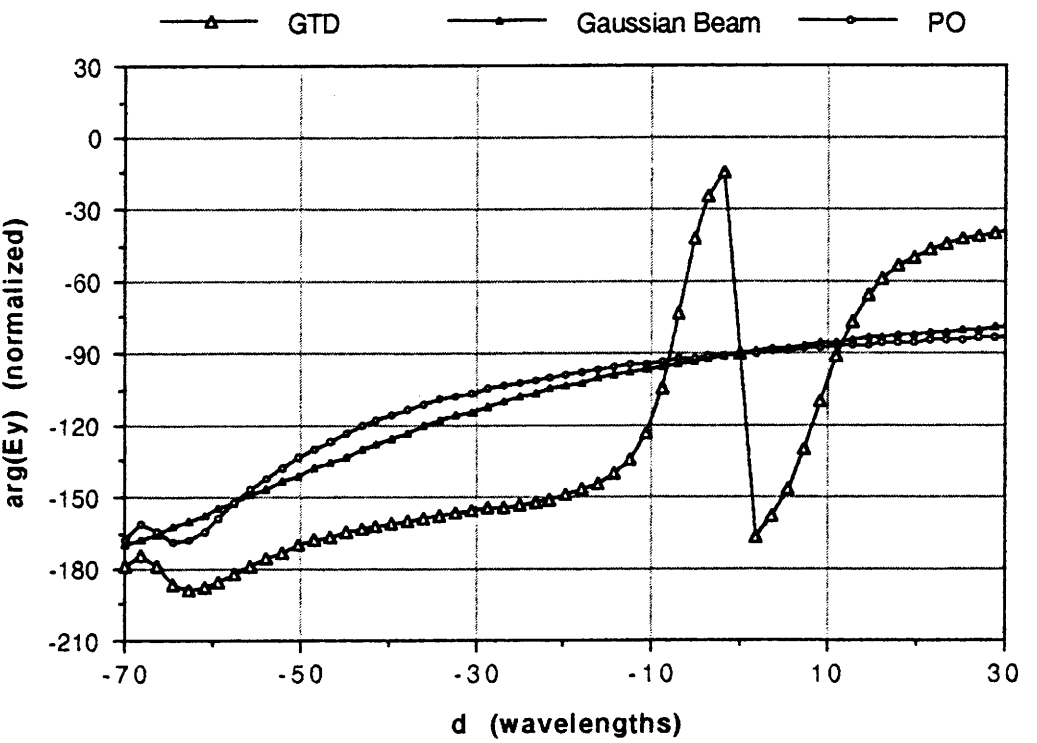
GTD
Gaussian Beam
PO
30
0
-30
-60
-90
-120
-150
-180
-210
arg(Ey) (normalized)
-70
-50
-30
-10
10
30
d (wavelengths)

Fig. 12

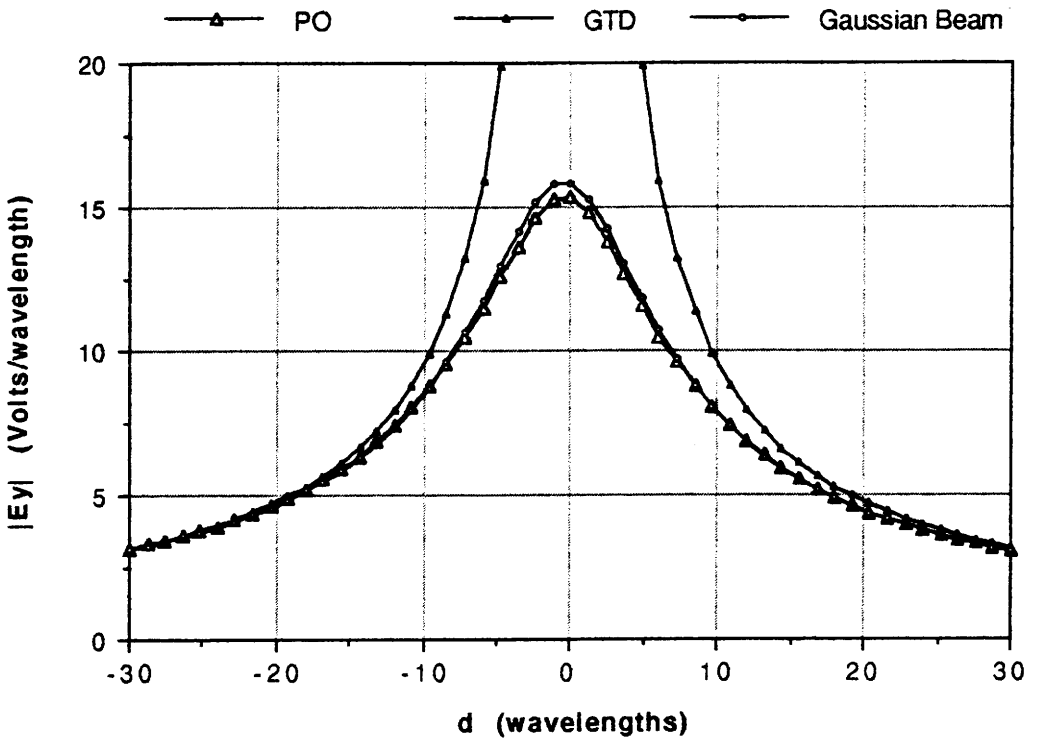
PO
GTD
Gaussian Beam
20
15
10
5
0
|Ey| (Volts/wavelength)
-30
-20
-10
0
10
20
30
d (wavelengths)

Fig. 13

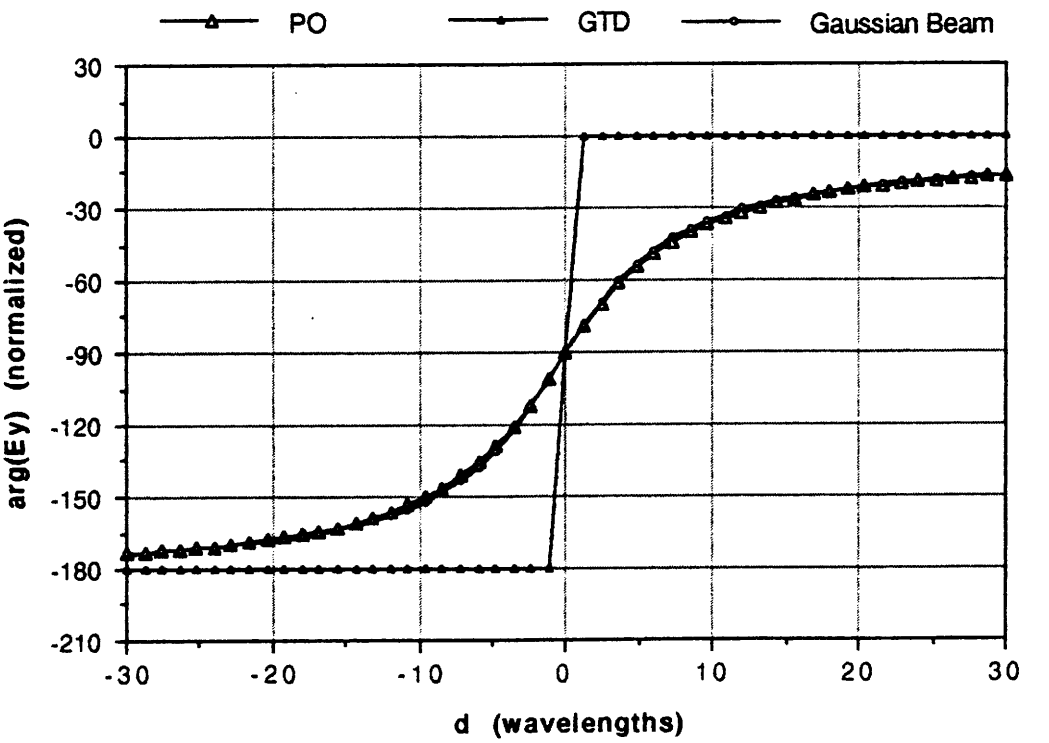
PO
GTD
Gaussian Beam
30
0
-30
-60
-90
-120
-150
-180
-210
arg(Ey) (normalized)
-30
-20
-10
0
10
20
30
d (wavelengths)

Fig. 14

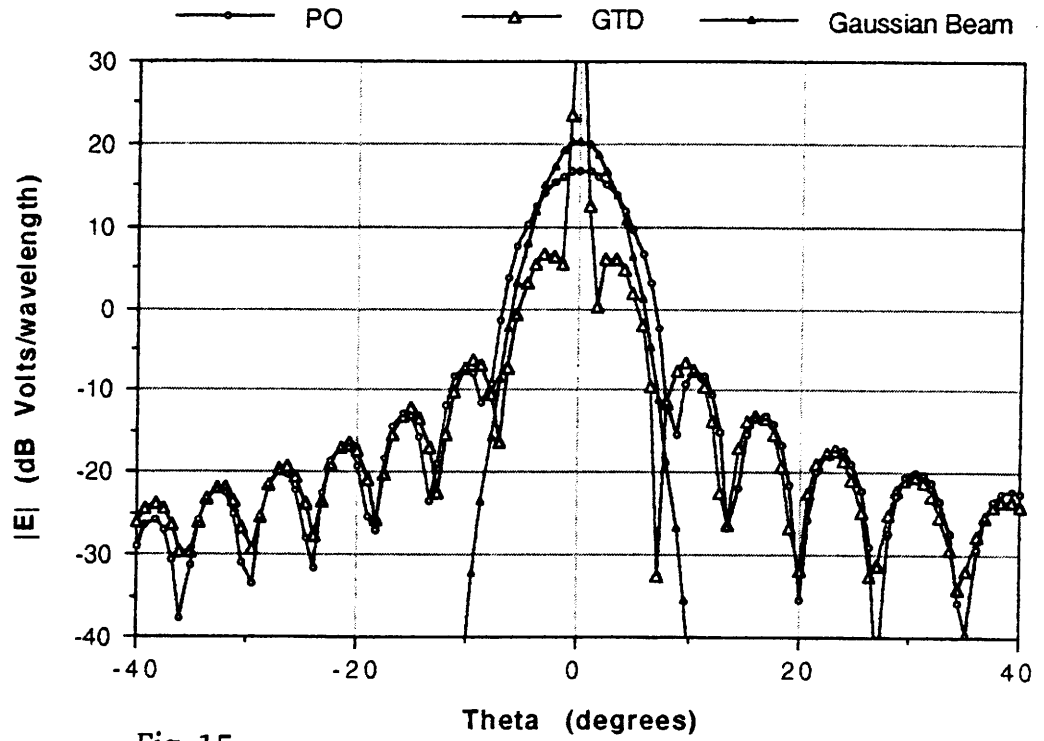
PO
GTD
Gaussian Beam
30
20
10
0
-10
-20
-30
-40
-40
-20
0
20
40
|E| (dB Volts/wavelength)
Theta (degrees)

Fig. 15

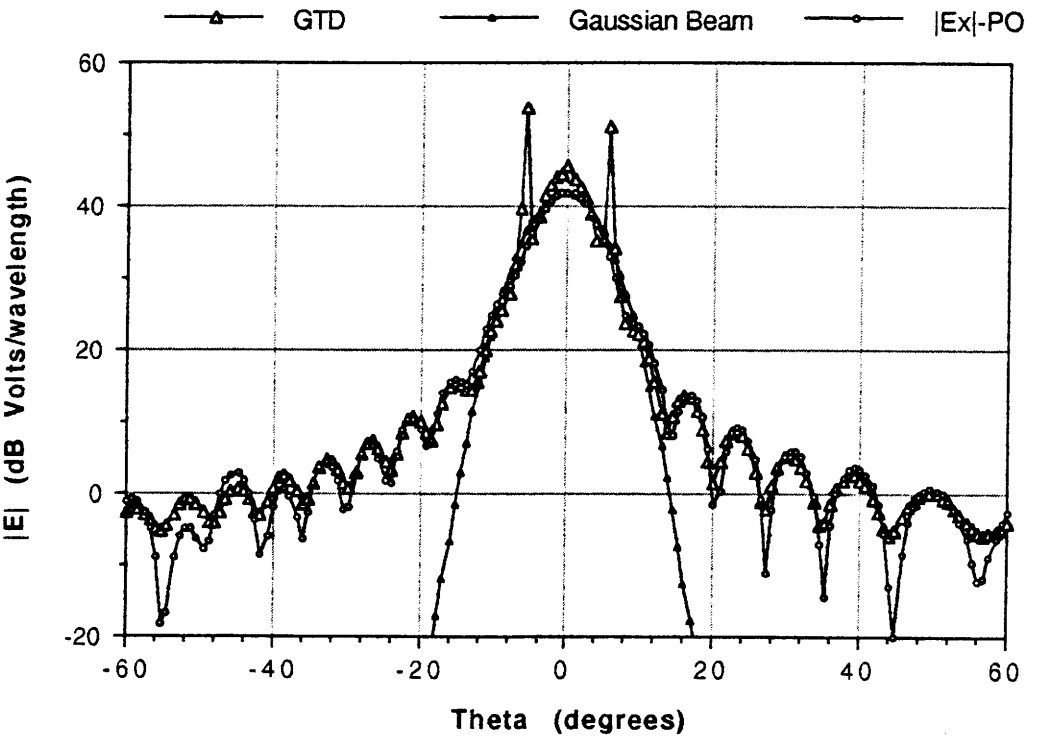
GTD
Gaussian Beam
|Ex|-PO
60
40
20
0
-20
-60
-40
-20
0
20
40
60
|E| (dB Volts/wavelength)
Theta (degrees)

Fig. 16

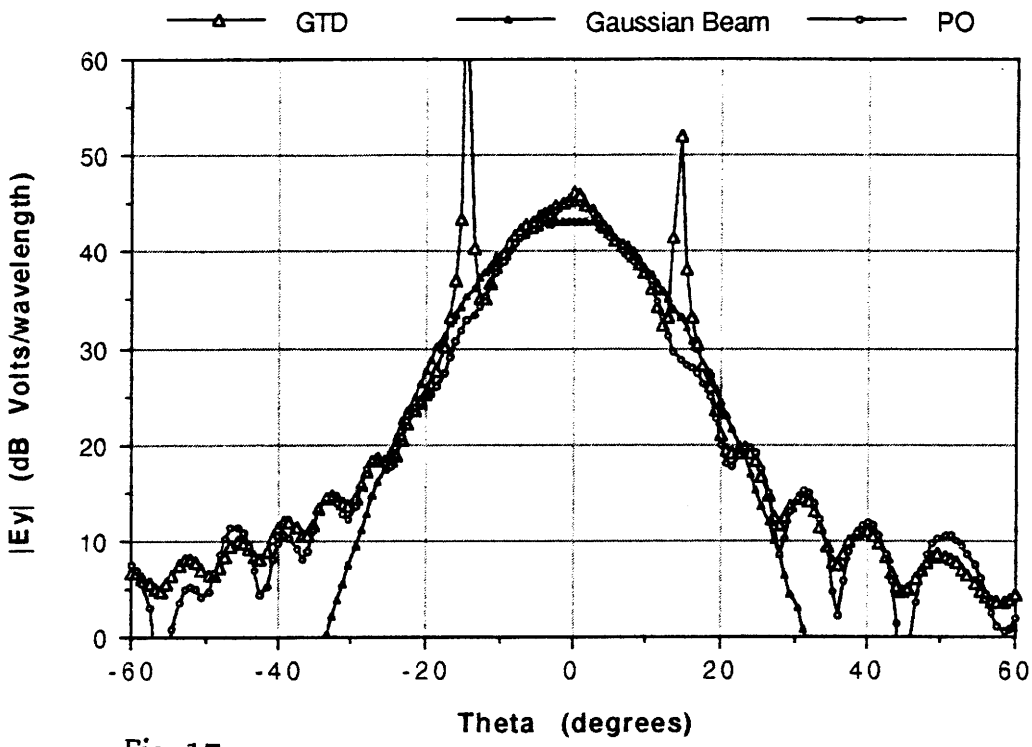
GTD
Gaussian Beam
PO
|Ey| (dB Volts/wavelength)
60
50
40
30
20
10
0
-60
-40
-20
0
20
40
60
Theta (degrees)

Fig. 17

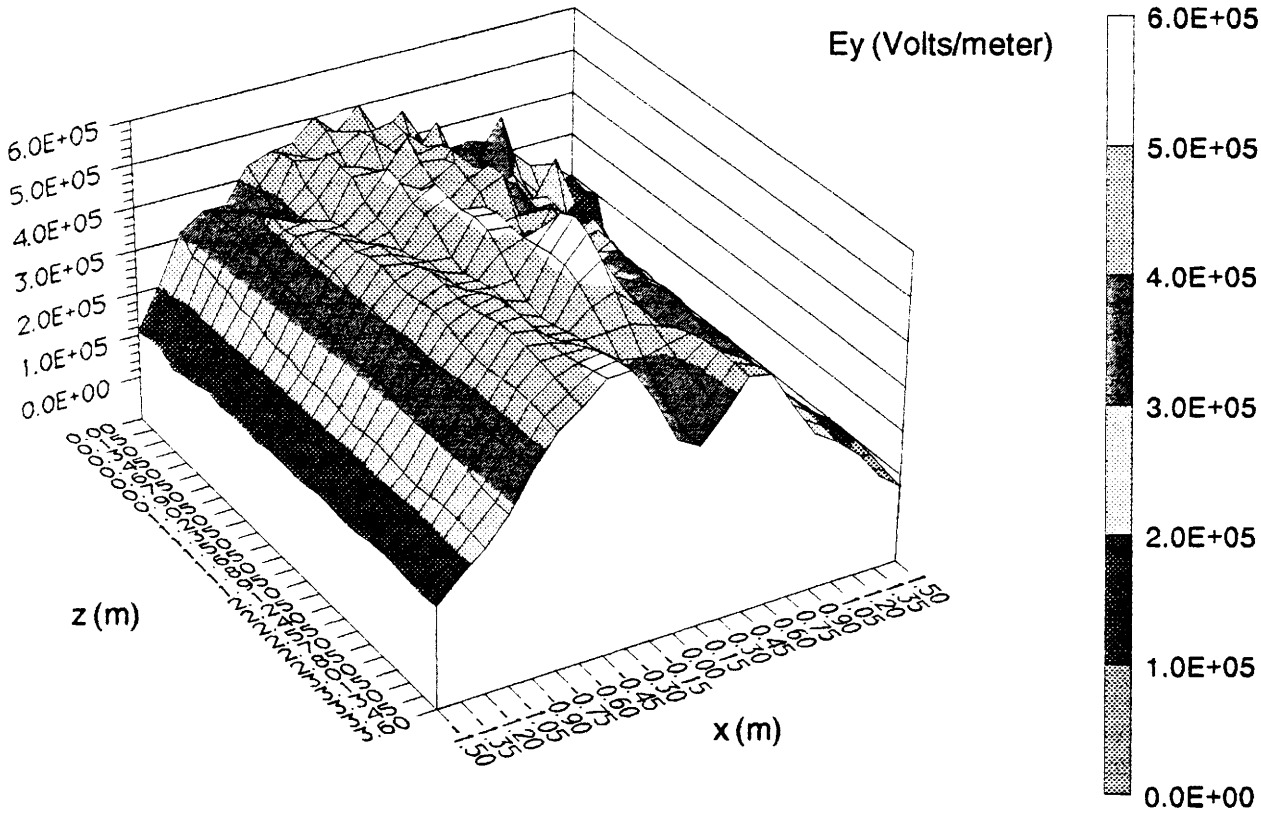
Ey (Volts/meter)
6.0E+05
5.0E+05
4.0E+05
3.0E+05
2.0E+05
1.0E+05
0.0E+00
z (m)
x (m)

Fig. 18

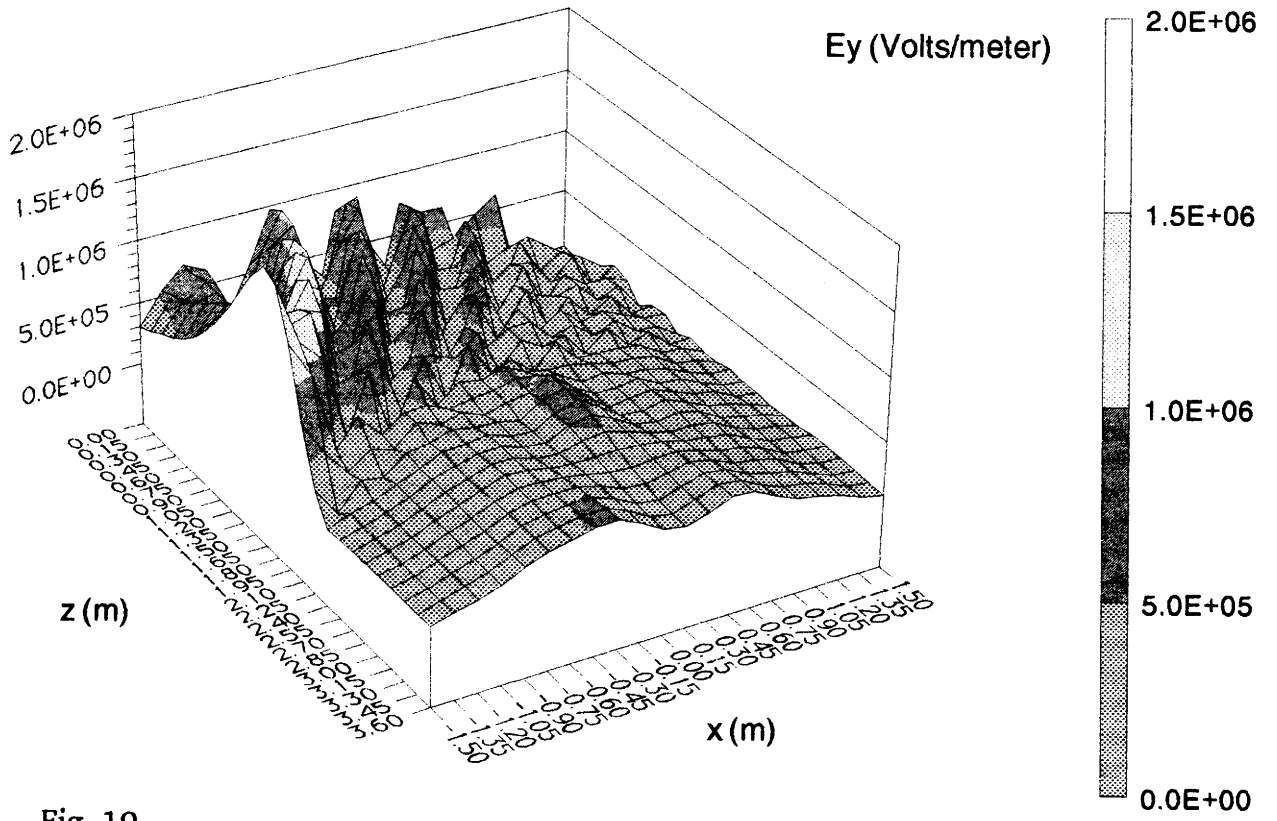

Fig. 19